Reliability Analysis Method for Soil Slopes Permanent Displacement under Mainshock-Aftershock Sequences

Tianyi Wang [a, b], Chengda Zhang [c*], Jiangwei Zhang [d*], Su Chen [e], Zhijun Dai [f*]

a. Key Laboratory of Intelligent Detection and Equipment for Underground Space of Beijing-Tianjin-Hebei Urban Agglomeration, Ministry of Natural Resources, Hebei GEO University, Shijiazhuang, 050031, China;
b. College of Earth Sciences, Hebei GEO University, Shijiazhuang, 050031, China;
c. 519 Team of North China Geological Exploration Bureau, Tianjin North China Geological Exploration Bureau, Baoding 071051, China;
d. State Key Laboratory of Hydroscience and Engineering, Tsinghua University, Beijing 100084, China;
e. Institute of Geophysics, China Earthquake Administration, Beijing 100081, China;
f. Key Laboratory of Urban Security and Disaster Engineering of the Ministry of Education, Beijing University of Technology, Beijing 100124, China.
Correspondence: Chengda Zhang (zcd_geo@163.com), Jiangwei Zhang (zhangjiangwei@tsinghua.edu.cn) and Zhijun Dai(dzj@cea-igp.ac.cn)

Abstract

After a primary seismic event, subsequent aftershocks frequently induce progressive damage to slopes. Evaluating the response of slopes to mainshock-aftershock sequences (MAS) from a probabilistic perspective is crucial for disaster prevention and mitigation. Current research primarily focuses on single mainshock events, and commonly adopts peak ground acceleration (PGA), with limited consideration of the cumulative aftershock effects. This study proposes a PDEM-based reliability framework for soil slopes subjected to MAS. First, the random input field of the MAS is first constructed by integrating theoretical models with real data. Then, taking into account the peak, cumulative, and spectral characteristics of the MAS, numerical simulations are performed to identify cumulative absolute velocity (CAV) among 21 candidate parameters as the controlling parameter for soil slope response. Finally, based on the probability density evolution method (PDEM), a reliability assessment framework for soil slope behavior under MAS is constructed. Compared with the existing methods, the proposed method reduces the dispersion of the displacement response by 37.5%–50% and raises the slope reliability by 5.3–14.5 percentage points at different displacement thresholds, thus accounting for aftershock characteristics and assessing the slope response with greater precision. This study offers approaches and methodologies for assessing slope stability under MAS from a probabilistic standpoint.

Keywords: mainshock-aftershock sequences, probability density evolution method, seismic response, soil slope, permanent displacement reliability

1 Introduction

Major seismic events are commonly followed by a series of aftershocks, whose effects on slope stability should not be underestimated. Actual seismic damage observations indicate that aftershocks often serve as the final trigger for overall failure of slopes (Xu and Huang, 2008; Yin, 2008). As safety requirements for engineering structures continue to escalate, slope stability under MAS has attracted considerable interest from researchers and practitioners alike. Li et al. (2009, 2017) pioneered and refined the PDEM framework for examining stochastic dynamic systems, establishing novel methodologies for nonlinear stochastic dynamic analysis and reliability evaluation of large-scale complex engineering structures. This framework demonstrates particular

* Corresponding author.
E-mail addresses: wangty@hgu.edu.cn (T. Wang), zcd_geo@163.com (C. Zhang), zhangjiangwei@mail.tsinghua.edu.cn (J. Zhang), chensuchina@126.com (S. Chen), dzj@cea-igp.ac.cn (Z. Dai).

effectiveness when applied to slope stochastic dynamic investigations. Expanding upon this foundation, Pang et al. (2021, 2024) introduced an enhanced generalized-PDEM approach for examining reliability in complex slope configurations. Their methodology encompasses multiple slope parameters alongside ground motion uncertainties. Additionally, accounting for the spatial variation in soil strength properties, a reliability assessment methodology integrating the Newmark method and PDEM is developed to evaluate the effects of aftershocks and spatial heterogeneity on slope dynamic reliability (Zhou et al., 2023; Wang et al., 2023; Xu et al., 2025). Contemporary investigations predominantly utilize peak ground acceleration (PGA) as the primary intensity metric. Nevertheless, within MAS contexts, maximum PGA typically manifests during the mainshock phase. Consequently, intensity parameters derived solely from peak values inadequately characterize the comprehensive ground motion attributes of MAS (Ruiz-Garcia and Negrete-Manriquez 2011; Amiri et al., 2022).

In terms of characterizing the ground motion random field of the MAS, the Monte Carlo method is a classic and effective means (Hu et al., 2018; Nithin et al., 2020; Kim and Sitar, 2013). However, it also has problems such as a large number of samples and incomplete probability information of the sample set (Jiang et al., 2021). The random function-dimension reduction simulation technique generates MAS time histories with associated probabilities, thereby establishing a complete probabilistic set. These histories can then be coupled with the PDEM to conduct sophisticated dynamic response and reliability analyses for complex engineering structures subjected to MAS (Liu et al., 2017; Liu et al., 2019; Liu et al., 2022).

Current reliability analysis methods for seismic slopes are predominantly designed for single-mainshock scenarios and thus cannot adequately perform reliability assessment under MAS. Moreover, existing studies on sequential ground motions predominantly use PGA as the intensity measure, which fails to capture the cumulative damage effect contributed by aftershocks. To address these limitations, this study adopts cumulative absolute velocity (CAV) as the intensity measure for MAS ground motions and, based on the PDEM, establishes a reliability analysis framework for the permanent displacement of soil slopes. The proposed method is capable of accounting for the influence of aftershocks, which can provide a reference for stability evaluation and disaster prevention of soil slopes subjected to MAS.

2 Methods

2.1 Model

This investigation employs a binary structural slope configuration to examine slope under the MAS. Fig. 1 shows the double-layer slope model established by referring to Wang et al. (2021). The dimensions of the model are 150 m in length and 30 m in height. Grid dimensions ΔL range from 0.5 m to 1.8 m, with a finer resolution of approximately 0.5 m in the potential sliding zone. The soil material is clay sourced from the southwestern region of China (Yang et al., 2022; Ma et al., 2023; Zhang et al., 2024), and its properties are detailed in Table 1.

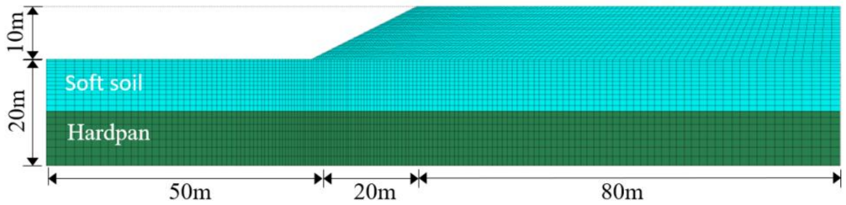

Fig. 1. Geometric dimensions and mesh division of the slope model

Table 1 Parameters of the slope

Soil layer	Density / (kg·m $^{-3}$)	Bulk modulus /MPa	Shear modulus /MPa	Cohesion /kPa	Internal friction angle /(°)	Shear strength /kPa
Soft soil	1900	70	37	34	24	4.2
Hardpan	2000	875	560	120	42	120

This investigation utilizes the finite-difference platform FLAC3D, with soil mechanical behavior characterized through a Mohr-Coulomb constitutive formulation incorporating tensile-cutoff provisions. Local damping is adopted in this study. Its implementation is given by Eq. (1) (Li et al., 2006). This computational strategy eliminates the need for global matrix assembly, thereby substantially reducing the time-step size. Such computational architecture enhances processing efficiency without compromising solution fidelity, rendering this methodology particularly appropriate for investigating nonlinear dynamic phenomena. (Hu et al., 2017; Puthanpurayil et al., 2018; Yan et al., 2011).

$$\xi = \pi D_s \tag{1}$$

Within Equation (1), the coefficient ξ quantifies localized damping intensity, Ds designates the critical damping fraction, while π maintains its conventional value of 3.14.

This investigation adopts a 5% critical damping fraction to replicate energy dissipation characteristics during seismic wave transmission through soil media (Qu et al., 2015), yielding a local damping coefficient of 0.157 according to Eq. (1).

2.2 Reliability analysis method of slope under MAS

Leveraging fundamental probability conservation principles, we may derive generalized density evolution equations applicable to stochastic dynamic system investigations. Integration with virtual stochastic process methodologies facilitates probabilistic modeling of stochastic datasets. Furthermore, based on the PDEM, the reliability analysis of the permanent displacement of the slope under the MAS action is realized (Li et al., 2008; Liu et al., 2017; Jiang et al., 2021). The main steps are as follows:

(1) The measured data of the MAS were statistically analyzed to obtain the frequency-domain energy distribution function curves of each ground motion. Employing optimal square approximation criteria, we determine the parameter vector λ defining each evolving power spectral density function. The MAS dataset in this research is modeled as zero-mean, fully non-stationary processes characterized by an evolutionary power spectral density (EPSD) model. The discrete representative points of each ground motion are expressed as $\theta_q = (\theta_{1,q}, \theta_{2,q}, \ldots, \theta_{s,q}$, $q = 1, 2, \ldots, 96)$, the discrete representative points assigned to probability for Eq. (2) :

$$P_q = \int_{V_q} p\Theta\,(\theta)d\theta \tag{2}$$

(2) Within the framework of reliability analysis based on PDEM, it is essential to identify a

ground-motion parameter that exhibits the strongest correlation with slope displacement responses for MAS events. We have demonstrated that among the 21 parameters evaluated across three categories—namely, peak types (PGA, PGV, PGD), spectral characteristics (Sa_{Ts}, $Sa_{1.5Ts}$, ASI), and cumulative types (a_{sq}, v_{sq}, d_{sq}, a_{rs}, v_{rs}, d_{rs}, I_A, CAV, CAD, CAI, a_{rms}, v_{rms}, d_{rms}, I_c, t_d)—CAV showed the highest correlation coefficient ($\rho = 0.872$) with the permanent displacement, and more effectively captured the characteristics of aftershocks, as shown in Fig. 2 (Zhang et al., 2024). Consequently, CAV is adopted as the governing parameter for slope displacement response under MAS, and is combined with the PDEM for reliability assessment.

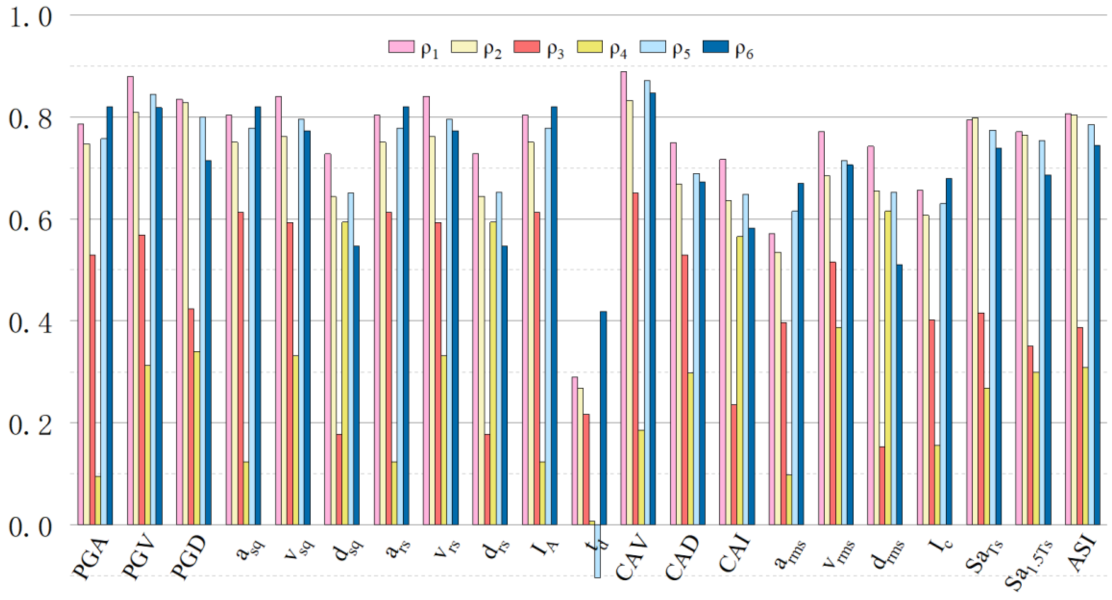

Fig. 2. Correlation coefficient of MAS ground motion parameters

Based on trial calculations, 96 sets of MAS were scaled to three CAV levels: 12 m/s, 28 m/s, and 40 m/s. Using the FLAC3D, the slope response under MAS, denoted as $\dot{X}_j(\Theta_q,t)$; j=1, 2, …, 96.

(3) Based on the above two steps to get assigned to probability P_q and slope of the response results $\dot{X}_j(\Theta_q,t)$ probability density evolution Eq. (3):

$$\frac{\partial p_{X\Theta}(x,\theta,t)}{\partial t} + \sum_{j=1}^{m}\dot{X}_j(\Theta_q,t)\frac{\partial p_{X\Theta}(x,\theta,t)}{\partial x} = 0,\ q=1, 2, 3, \ldots\ldots, 96 \tag{3}$$

Within this formulation, X designates system response quantities, Θ encompasses the ensemble of random variables exclusive of initial conditions. $\Theta = (X_0, \dot{\Theta})$ represents the vector comprising all stochastic variables within the system; $X = H(\Theta, t)$ indicates the physical response of X; $p_{X\Theta}(x,\theta,t)$ signifies the joint probability density function (PDF) for X and Θ.

When $t = t_0$, the following initial condition is as shown in Eq. (4):

$$p_{X\Theta}(x,\theta,t)|_{t=t_0} = \delta(x - x_0)\, P_\Theta(\theta) \tag{4}$$

In this expression, δ denotes the Dirac delta function, while x_0 corresponds to the X value $t = t_0$. The PDF of X at any given time can be derived by accumulating all discrete numerical solutions, as expressed in Eq. (5):

$$p_X(x,t) = \int p_{X\Theta}(x,\theta,t)d\theta \tag{5}$$

Probability density evolution equations necessitate numerical solution methodologies. Direct analytical solution derivation for Eq. (5). presents considerable mathematical complexity. Conventional practice employs finite difference approximations for solution advancement.

$$\frac{\partial p(z,t)}{\partial t} + a(\,t)\frac{\partial p(z,t)}{\partial z} = 0 \tag{6}$$

First-order Taylor series expansion of Eq. (6), yields approximate differential expressions:

$$\left[\frac{\partial p}{\partial t}\right]_j (k) = \frac{p_j^{(k+1)} - p_j^{(k)}}{\Delta t} \tag{7}$$

For spatial coordinate z, analogous treatment produces:

$$\left[\frac{\partial p}{\partial z}\right]_j (k) = \frac{p_j^{(k+1)} - p_j^{(k)}}{\Delta z} \tag{8}$$

Substitute Eqs. (7) and (8) into Eq. (6):

$$p_j^{(k+1)} = p_j^{(k)} - \lambda a^{(k)}\left[p_j^{(k)} - p_{j-1}^{(k)}\right] \text{ or } p_j^{(k+1)} = \left(1 - \lambda a^{(k)}\right)p_j^{(k)} + \lambda a^{(k)} p_{j-1}^{(k)} \tag{9}$$

Eq. (9) is the one-sided difference scheme. Substitute $\dot{X}_j\left(\Theta_q, t\right)$ obtained from ② into Eq. (3), and solve the partial differential equation using the L-W or TVD format of the finite difference method.

(4) The PDF of slope displacement response $p\_X(x,t)$ is obtained numerically through cumulative summation of the joint PDF $p\_X\Theta(x,\theta,t)$; $q = 1, 2, \ldots, 96$. Subsequently, plots of the PDF and cumulative distribution function (CDF) are generated for the slope displacement. The statistical properties of the displacement datasets are visualized via these plots, which serve as the basis for assessing slope reliability.

3 Stochastic simulations of MAS

Empirical MAS recordings furnish superior fidelity representations of structural damage phenomenology and cumulative degradation mechanisms (Yang et al., 2022). This study employs diverse real seismic records to mitigate bias arising from any specific ground-motion type. By iteratively identifying parameters within an evolutionary power spectral density framework, it integrates theoretical principles with data-driven approaches to derive stochastic seismic input representations. This offers a stochastic loading source for studying how MAS affect slope reliability.

This investigation selected 96 authentic mainshock–aftershock pairs from 15 seismic events in the NGA-West2 strong-motion database of the Pacific Earthquake Engineering Research Center (PEER). We selected records based on five criteria (Bray and Macedo, 2019; Yeznabad et al., 2022): (1) the mainshock and its aftershock must belong to the same seismic event, with the aftershock defined as the largest-magnitude event occurring within 12 months after the mainshock; (2) both events have a $Mw \geq 5.0$ and a PGA ≥ 0.05 g; (3) both records are taken from the same component of the same station; (4) the station has an 30-meter average shear wave velocity between 100 and 700 m/s; and (5) the rupture distance of each event does not exceed 80 km. We used real earthquake records in this study, preserving the natural amplitude and frequency characteristics of the ground motions. This approach avoids introducing biases associated with amplitude scaling.

Each MAS assembly adopted a "mainshock + 20-second temporal gap + aftershock" configuration to preserve comprehensive non-stationary sequence characteristics (Wang et al., 2023). Fig. 3 displays a typical mainshock–aftershock acceleration record from the Whittier Narrows event, with the mainshock and aftershock numbered 589 and 707, respectively, in the NGA-West2 database.

For the mainshock-aftershock sequential ground motion assemblies constructed above, frequency-domain energy distribution investigations proceed utilizing evolutionary power spectrum modeling of fully non-stationary ground motion processes (Priestley, 1965; Liu et al., 2017). The energy distribution curve in the frequency domain is fitted by applying the least squares method, following the best square approximation criterion. The parameter vector λ is further obtained through inversion and regression. In the process, considering the site damping ratio ξ_f excellence, site soil circular frequency ω_f and the influence of a frequency modulation function parameter. The identification results are shown in Fig. 4, and the data results are presented in Table 2. In the constructed earthquake, it can be regarded as a zero-mean real non-stationary ground motion process generated by the evolving power spectral density function model.

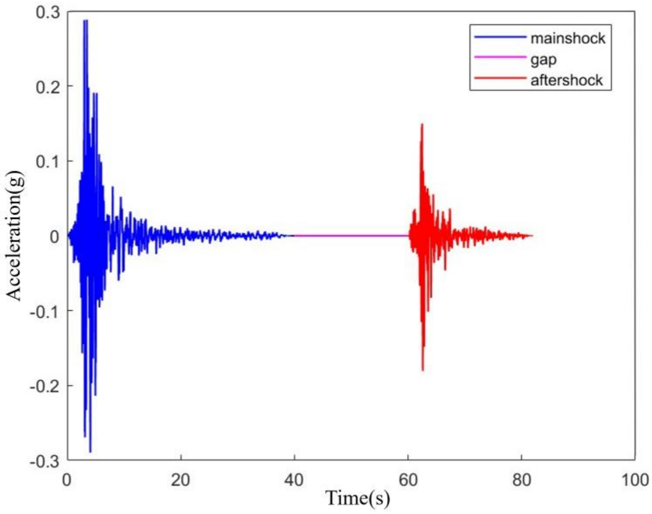

Fig. 3. Typical acceleration time history of a MAS

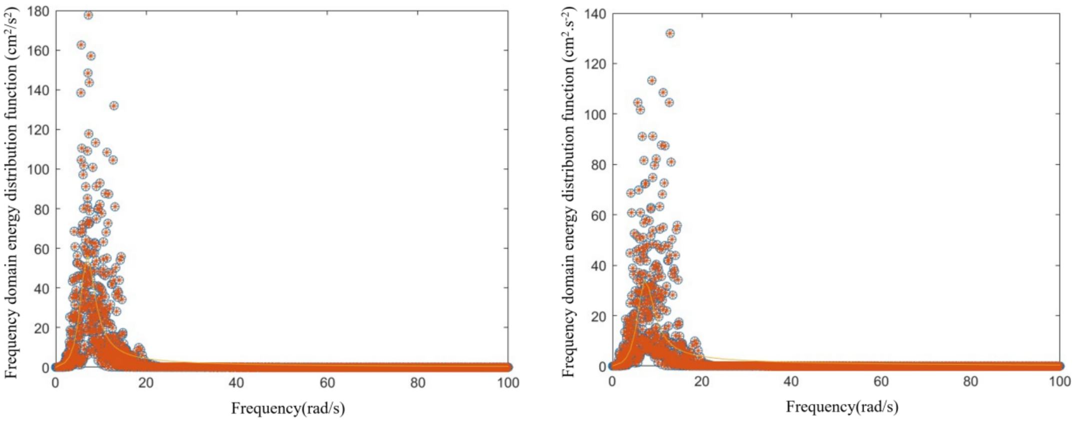

（a）the fitting results of the mainshock　　（b）The fitting results of the aftershock

Fig. 4. The identification effect of the parameter vector λ

Table 2 Identification results of MAS

Earthquake type	Damping ratio	Superior circular frequency	Time−frequency modulation function
mainshock	0.32	14.09	0.64
aftershock	0.37	14.64	0.71

4 Results and analysis

To assess slope reliability based on permanent displacement outcomes, defining critical stability states proves necessary. Jibson and Michael (2009) classified slope displacement into four ranges for seismic landslide risk evaluation: displacements of 0-0.01m indicate low risk, 0.01-0.05m suggest medium risk, 0.05-0.15m represent high risk, and those exceeding 0.15m denote very high risk. For permanent displacement, Yener (1988) suggests that the control standard for seismic sliding deformation is 1m. In this study, combined with the actual engineering requirements, three slope displacement thresholds of 0.05m, 0.25m and 0.50m were selected, corresponding to three failure degrees of low, medium and high respectively, to systematically evaluate the reliability of slope displacement under the MAS action.

Fig. 5 shows the distribution of the slope permanent displacement under the MAS. The distribution has a large degree of dispersion, and with the increase of ground motion intensity, the displacement response of the slope also increases. When the CAV of the MAS was 12m/s, 28m/s and 40m/s respectively, the permanent displacements of the slope were 0.067m, 0.328m and 0.633m respectively, which were like the slope displacement results when the PGA of the MAS was 0.4g, 0.5g and 0.6g in reference (Wang et al., 2023). The difference is that the discreteness degree of the permanent displacement of the slope obtained in this study becomes smaller. With the increase of the CAV, the slope displacement response results are increasingly concentrated around the average value. This tendency substantiates CAV superiority relative to the commonly used PGA as the characterization parameter for MAS when investigating slope displacement reliability.

Nevertheless, even with the use of CAV as the characterizing parameter, the obtained slope displacement responses remain somewhat scattered. This suggests that additional ground-motion parameters—including frequency content and duration—also play a role in influencing slope displacement (Rathje and Saygili, 2008; 2009; Yeznabad et al.,2022) Given the current lack of a single comprehensive ground-motion parameter that can effectively predict slope displacement responses, the PDEM framework propagates this inherent variability into the reliability estimate, thus rendering a probabilistic treatment indispensable. Building on previous studies, the present study introduces a reliability probabilistic analysis method that integrates the PDEM.

Fig. 6 delineates PDF and CDF curves characterizing slope displacement. PDF curves reveal the clustering patterns and variation extents within displacement datasets, thus presenting the distributional features of slope movement data in a visual manner. The CDF curve determines the cumulative probability of displacement and is used to evaluate the reliability of the permanent displacement of the slope. The PDF for slope displacement shown in Fig. 5 display bimodal or multimodal patterns, making it difficult to describe them using standard distributions like normal or lognormal models. Under the MAS action of different intensities, the displacements of slopes have diverse distribution patterns, and their probabilities are also not the same. When the CAV is 12 m/s, the fluctuation span of slope displacement response ranges from 0-0.25m. Under a low failure degree with a displacement threshold of 0.05 m, the reliability of the slope is 48.5%. With the growth of CAV, the variation range of slope displacement response under the MAS keeps expanding, while the concentrated area of permanent displacement becomes wider. When the CAV is 28 m/s, the fluctuation span of slope displacement response extends from 0 m to 1 m, mainly concentrated between 0-0.5 m. Under the medium failure degree with the displacement threshold of 0.25 m, the reliability of the slope is 45.5%. When the CAV is 40 m/s, the fluctuation span of slope displacement response spans from 0 to 2 m, mainly concentrated between 0-1 m. Under the high failure degree with a displacement threshold of 0.5m, the slope's reliability reaches 31.7%.

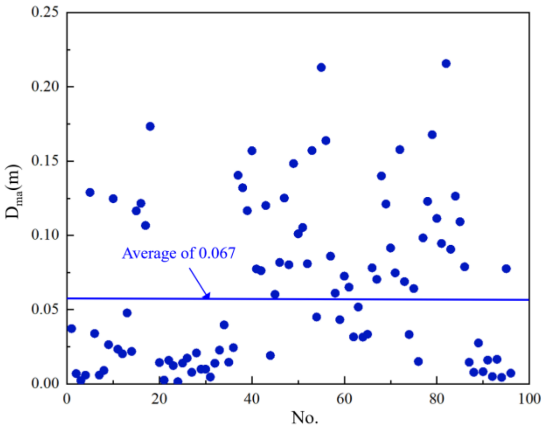

(a) displacement distribution map when CAV = 12 m/s

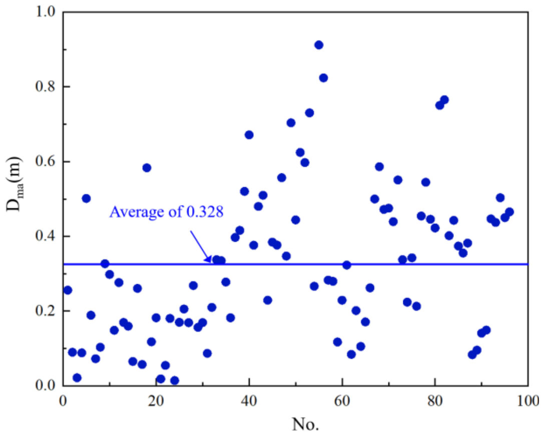

(b) Displacement distribution map when CAV = 28 m/s

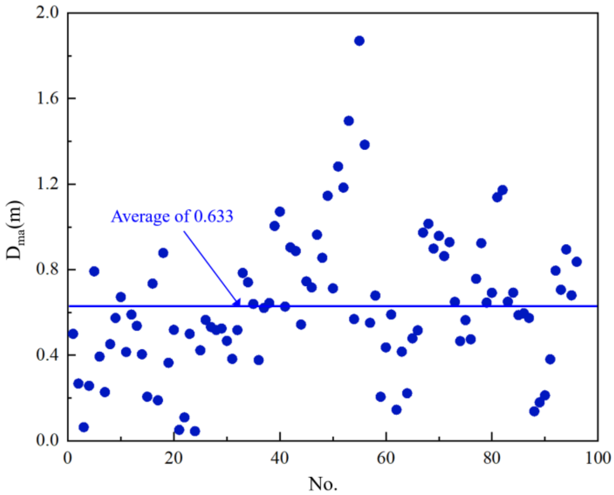

(c) displacement distribution map when CAV = 40 m/s

Fig. 5. displacement response distribution of slopes under mas

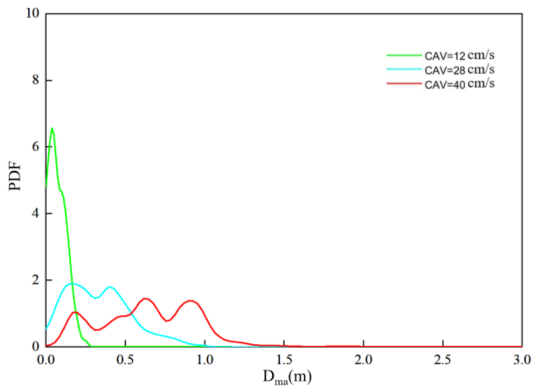

(b) PDF

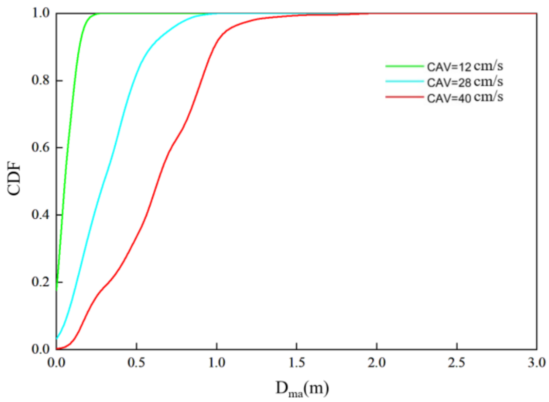

(b) CDF

Fig. 6. Statistical analysis of slope displacement response probability under MAS

This investigation's outcomes undergo comparative evaluation against conventional slope displacement reliability analysis results, which customarily employ PGA as the seismic ground motion parameter (Wang et al., 2023), as depicted in Fig. 7-9. Fig. 7 shows that adopting CAV as the seismic ground-motion parameter leads to a tighter distribution of slope displacement, with the displacement range narrowed by 37.5%–50%, fewer outliers, and more precise response estimation. Figures 8 and 9 further indicate that, compared with PGA, CAV consistently yields higher slope reliability across all damage thresholds: at 0.05 m, reliability rises from 39.2% to 48.5% (+9.3 pp); at 0.5 m, from 76.7% to 82.0% (+5.3 pp); and at 1 m, from 77.2% to 91.7% (+14.5 pp). These results demonstrate that using CAV as the seismic intensity control parameter for sequence-type ground motions can more effectively evaluate slope reliability.

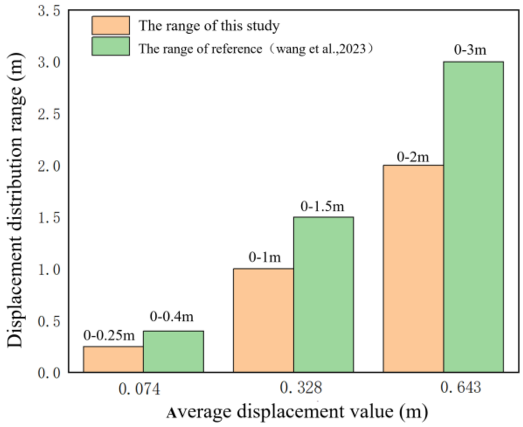

Fig. 7. Comparison of slope displacement response distribution

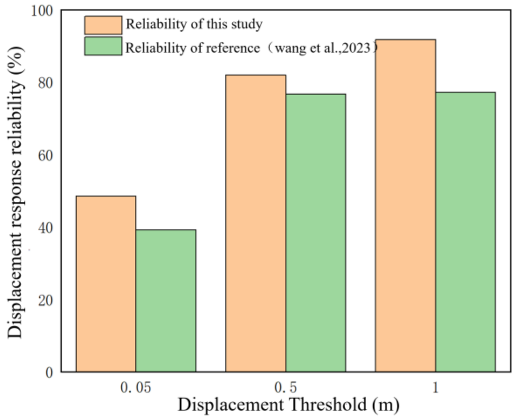

Fig. 8. Comparison of slope displacement reliability

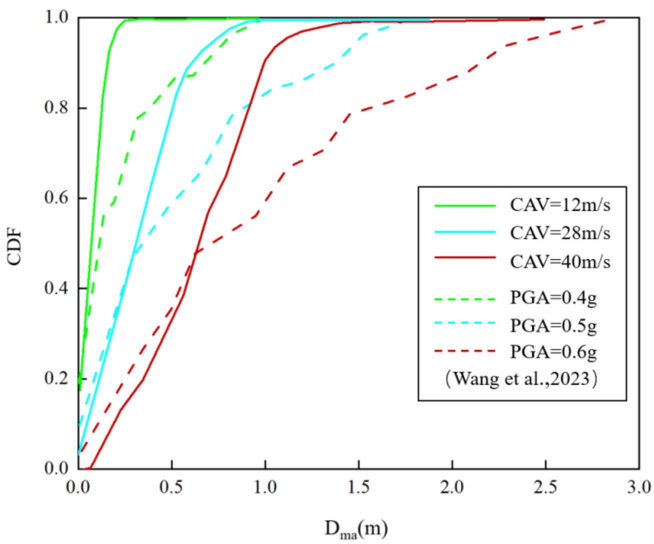

Fig. 9. Compared with the reliability results of slope displacement response in reference

5 Conclusions

By studying the intensity-controlling parameters of the MAS in soil slope responses and based on PDEM, an assessment methodology addressing slope reliability under MAS excitations is presented herein. Benchmarking against conventional techniques reveals the following insights:

(1) Among 21 distinct MAS parameter types, CAV showed the strongest correlation with the permanent displacement (ρ = 0.872) and best represents the cumulative effects of MAS. Therefore, CAV can be used as the optimal parameter to assess the response of soil slopes under the MAS action.

(2) Based on the dynamic calculation results, as CAV increases from 12 m/s to 40 m/s, the slope displacement response gradually increases, while the displacement results still exhibit a degree of scatter. Consequently, employing probabilistic analysis methodologies becomes essential when

evaluating soil slope stability under MAS loading.

(3) By incorporating MAS characteristics and utilizing PDEM, a methodology for computing slope displacement response reliability under MAS has been established. Compared with the conventional PGA-based approach, this method reduces the dispersion of the displacement response by 37.5%–50% and raises the slope reliability by 5.3%–14.5 % at the different thresholds, which has both theoretical significance and practical engineering value.

It is worth pointing out that this study focuses on clayey soil slopes in the southwestern region of China, with an emphasis on the feasibility of the reliability analysis method for soil slope response under the crustal MAS action. The study does not consider the variability of soil parameters and the slope geometry. The principal contribution of this work lies in the methodological framework, specifically the integration of CAV as the intensity measure for MAS with the PDEM for efficient reliability analysis. Considering the variability of soil parameters will be of great significance to practical engineering applications.

Code and data availability. The MAS ground motions in this study was based on the NGA-West2 strong-motion database from the Pacific Earthquake Engineering Research Center.

Author contributions. JZ and CZ designed the research and optimized the overall structure of this paper. TW and CZ completed most of the main work, including the programming, debugging of parameters, and final drafting of the article. SC and ZD contributed some important algorithm ideas and completed the work of the comparison part. JZ and CZ provided the original algorithm ideas and framework for this study and provides valuable suggestions for program optimization and parameter adjustment.

Competing interests. The contact author has declared that none of the authors has any competing interests.

Disclaimer. Views and opinions expressed are, however, those of the author(s) only and do not necessarily reflect those of the European Union or REA. Neither the European Union nor the granting authority can be held responsible for them.

Publisher's note. Copernicus Publications remains neutral with regard to jurisdictional claims made in the text, published maps, institutional affiliations, or any other geographical representation in this paper. While Copernicus Publications makes every effort to include appropriate place names, the final responsibility lies with the authors. Views expressed in the text are those of the authors and do not necessarily reflect the views of the publisher.

Financial support. This work was supported by the financial support from the National Natural Science Foundation of China (Grant Nos. 51908176, 62273315 and 52192675). These financial supports are gratefully acknowledged.

Review statement.

References

Amiri, S., Di Sarno, L., Garakaninezhad, A., 2022. Correlation between non-spectral and cumulative-based ground motion intensity measures and demands of structures under mainshock-aftershock seismic sequences considering the effects of incident angles. Structures 46, 1209–1223. https://doi.org/10.1016/j.istruc.2022.05.033

Bray, J. D., Macedo, J., 2019. Procedure for estimating shear-induced seismic slope displacement for shallow crustal earthquakes. J. Geotech. Geoenviron. Eng. 145 (12), 04019106. https://doi.org/10.1061/(ASCE)GT.1943-5606.0002143

Hu, C. B., Wang, Y. G., Ling, D. S., 2017. Physical essence and influence of model parameters on dynamic response of Rayleigh damping. J. Zhejiang Univ. (Eng. Sci.) 51 (7), 1284 - 1290. https://doi.org/10.3785/j.issn.1008 - 973X.2017.07.003.

Hu, S., Gardoni, P., Xu, L., 2018. Stochastic procedure for the simulation of synthetic mainshock-aftershock ground motion. Earthquake Eng. Struct. Dyn. 47 (11), 2275–2296. https://doi.org/10.1002/eqe.3026

Jiang, Y., Ruan, X., Liu, Z., 2021. Dimension-reduction simulation of main-aftershock type ground motion process. J. Vib. Shock 40 (24), 282–292.

Jibson, R.W., Michael, J.A., 2009. Maps showing seismic landslide hazards in Anchorage, Alaska. Washington, DC: USGS. https://doi.org/10.3133/sim3077

Li J, Chen J. The principle of preservation of probability and the generalized density evolution equation[J]. Structural Safety, 2008, 30(1): 65-77.

Li, J., Chen, J., 2017. Some new advances in the probability density evolution method. Appl. Math. Mech. 38 (1), 32–43. https://doi.org/10.1007/s10778-017-0084-2

Li, J., Liu, Z., Chen, G., 2009. Orthogonal expansion of ground motion and PDEM-based seismic response analysis of nonlinear structures. Earthq. Eng. Eng. Vibration 8, 313–328. https://doi.org/10.1007/s11803-009-9090-8

Li, S. H., Yang, S. P., 2006. Research status of hysteretic nonlinear models. J. Dyn. Control 4 (1), 8 - 15. https://doi.org/10.3969/j.issn.1672 - 6553.2006.01.003.

Liu, Z., Jiang, Y., Liu, Z., Ruan, X., 2022. Dimension-reduction simulation of main-aftershock type vector process based on strong motion records. Earthq. Eng. Eng. Dyn. 42 (4), 179–190. https://doi.org/10.13197/j.eeed.2022.0420

Liu, Z., Liu, Z., 2017. Simulation of fully non-stationary ground motion based on seismic design response spectrum. J. Vib. Eng. 30 (3), 457–465. (in Chinese)

Liu, Z., Liu, Z., Ruan, X., et al., 2019. POD-based dimension reduction representation of stochastic ground motion fields. Sci. Sin. Technologica 49 (5), 589–601. (in Chinese)

Ma, Z. G., Zhu, B. L., Wu, H. G., et al., 2023. Experimental study on seismic failure characteristics optimization of landslide - tunnel shock absorption based on energy analysis. Chin. J. Rock Mech. Eng. 42 (04), 879 - 895. https://doi.org/10.13722/j.cnki.jrme.2022.0516.

Nithin, V. L., Das, S., Kaushik, H. B., 2020. Stochastic simulation of fully nonstationary aftershock ground motions from known preceding mainshock. Soil Dyn. Earthq. Eng. 130, 1–11. https://doi.org/10.1016/j.soildyn.2020.105968

Pang, R., Xu, B., Zhou, Y., et al., 2021. Seismic time-history response and system reliability analysis of slopes considering uncertainty of multi-parameters and earthquake excitations. Comput. Geotech. 136, 104245. https://doi.org/10.1016/j.compgeo.2021.104245

Pang, R., Yao, H., Xu, M., et al., 2024. Slope displacement reliability analysis considering rock parameters spatial variability subjected to stochastic mainshock-aftershock earthquake. Reliab. Eng. Syst. Saf. 251, 110337. https://doi.org/10.1016/j.ress.2023.110337

Priestley, M. B., 1965. Evolutionary spectra and non - stationary processes. J. R. Stat. Soc. Ser. B (Methodol.) 27

(2), 204 - 229.

Puthanpurayil, A. M., Lavan, O., Carr, A. J., et al., 2018. Application of local elasticity continuum damping models in nonlinear dynamic analysis. Bull. Earthquake Eng. 16, 6365 - 6391. https://doi.org/10.1007/s10518 - 018 - 0424 - 7.

Qu, H. L., Hu, H. G., Zhang, J. J., Zhu, D. P., 2015. Dynamic response characteristics of anchor cable piles under ground motion. China Earthq. Eng. J. 37 (02), 317 - 323. https://doi.org/10.3969/i.issn.1000 - 0844.2015.02.0317.

Rathje, E. M., Saygili, G., 2008. Probabilistic seismic hazard analysis for the sliding displacement of slopes: scalar and vector approaches. J. Geotech. Geoenviron. Eng. 134 (6), 804–814. https://doi.org/10.1061/(ASCE)1090-0241(2008)134:6(804)

Ruiz-Garcia, J., Negrete-Manriquez, J. C., 2011. Evaluation of drift demands in existing steel frames under as-recorded far-field and near-fault mainshock-aftershock seismic sequences. Eng. Struct. 33 (2), 621–634. https://doi.org/10.1016/j.engstruct.2010.12.006

Rathje, E. M., Saygili, G., 2009. Probabilistic assessment of earthquake-induced sliding displacements of natural slopes. Bull. N. Z. Soc. Earthq. Eng. 42 (1), 18–27. https://doi.org/10.5459/bnzsee.42.1.18-27

Xu Q, Huang R Q. Preliminary study on dynamic characteristics of large-scale landslide hazards induced by the 5.12 Wenchuan earthquake[J]. Journal of Engineering Geology, 2008, 16(06): 721-729.

Xu, B., Wang, G., Pang, R., 2025. Dynamic reliability analysis of slopes considering material parameter spatial variability under mainshock-aftershock sequences. J. Civ. Environ. Eng. (in Chinese)

Wang, G., Pang, R., Yu, X., et al., 2023. Permanent displacement reliability analysis of soil slopes subjected to mainshock-aftershock sequences. Comput. Geotech. 153, 105069. https://doi.org/10.1016/j.compgeo.2023.105069

Wang, W., Li, D. Q., Liu, Y., et al., 2021. Influence of ground motion duration on the seismic performance of earth slopes based on numerical analysis. Soil Dyn. Earthq. Eng. 143, 106595. https://doi.org/10.1016/j.soildyn.2021.106595.

Yan, Z. H., Zhang, S., Zhang, X. D., Zhang, L. P., 2011. Study of dynamic response of bedding rock slope under earthquake and influence of ground motion parameters. Chin. J. Rock Mech. Eng 30 (S2), 3522 - 3528. https://doi.org/CNKI:SUN:YSLX.0.2011- S2 - 022.

Yang, C. W., Zhang, L., Dong, L. J., et al., 2022. Research on the difference of dynamic responses between bedding and toppling rock slopes based on shaking table test. Chin. J. Rock Mech. Eng. 41 (02), 271 - 281. https://doi.org/10.13722/j.cnki.jrme.2021.0168.

Yener Ozkan, M., 1998. A review of considerations on seismic safety of embankments and earth and rock-fill dams. Soil Dyn. Earthq. Eng. 17 (7-8), 439–458. https://doi.org/10.1016/S0267-7261(98)00035-9

Yeznabad, A. F., Assatourians, K., El Naggar, M. H., & Molnar, S. (2022). Evaluation of earthquake-induced slope displacements in Greater Vancouver based on probabilistic framework and using NBCC 2020 and EqDisp code platform. *Earthquake Spectra*. https://doi.org/10.1002/esp4.70060

Yeznabad, A. F., Molnar, S., El Naggar, M. H., et al., 2022. Estimation of probabilistic seismic sliding displacement and pseudo-static coefficients (k15) for seismic stability assessment of slopes in the southern Lower Mainland, British Columbia. Soil Dyn. Earthq. Eng. 161, 107364. https://doi.org/10.1016/j.soildyn.2022.107364

Yin Y P. Research on geological hazards induced by the Wenchuan M8.0 earthquake[J]. Journal of Engineering Geology, 2008(04): 433-444.

Zhang, C., Zhang, J., Chen, S., et al., 2024. Response characteristics of soil slope under mainshock–aftershock sequences–type ground motions: Incremental damage effect, polarity effect, and correlation. Soil Dyn. Earthq. Eng. 187, 108940. https://doi.org/10.1016/j.soildyn.2023.108940.

Zhou, H., Wang, G., Yu, X., Pang, R., 2023. Dynamic reliability analysis of layered slope considering soil spatial variability subjected to mainshock-aftershock sequence. Water 15 (8), 1540. https://doi.org/10.3390/w15081540